Molecular organization of nematic liquid crystals between concentric cylinders: Role of the elastic anisotropy

C. Chiccoli,[1] P. Pasini,[1] L. R. Evangelista,[2] R. T. Teixeira-Souza,[3,*] and C. Zannoni[4]

[1]*Istituto Nazionale di Fisica Nucleare, Sezione di Bologna, Via Irnerio 46, 40126 Bologna, Italy*
[2]*Departamento de Física, Universidade Estadual de Maringá, Avenida Colombo, 5790-87020-900 Maringá, Paraná, Brazil*
[3]*Universidade Tecnológica Federal do Paraná, Campus Apucarana, Rua Marcílio Dias 635, 86812-460 Apucarana, Paraná, Brazil*
[4]*Dipartimento di Chimica Industriale "Toso Montanari" and INSTM, Università di Bologna, Viale Risorgimento 4, 40136 Bologna, Italy*

The orientational order in a nematic liquid crystal sample confined to an annular region between two concentric cylinders is investigated by means of lattice Monte Carlo simulations. Strong anchoring and homeotropic orientations, parallel to the radial direction, are implemented at the confining surfaces. The elastic anisotropy is taken into account in the bulk interactions by using the pair potential introduced by Gruhn and Hess [T. Gruhn and S. Hess, Z. Naturforsch. A **51**, 1 (1996)] and parametrized by Romano and Luckhurst [S. Romano, Int. J. Mod. Phys. B **12**, 2305 (1998); Phys. Lett. A **302**, 203 (2002); G. R. Luckhurst and S. Romano, Liq. Cryst. **26**, 871 (1999)], i.e., the so-called GHRL potential. In the case of equal elastic constants, a small but appreciable deformation along the cylinder axis direction is observed, whereas when the values of K_{11}/K_{33} if $K_{22} = K_{33}$ are low enough, all the spins in the bulk follow the orientation imposed by the surfaces. For larger values of K_{11}/K_{33}, spontaneous deformations, perpendicular to the polar plane, increase significantly. Our findings indicate that the onset of these deformations also depends on the ratio K_{22}/K_{33} and on the radius of the cylindrical surfaces. Although expected from the elastic theory, no tangential component of the deformations was observed in the simulations for the set of parameters analyzed.

　　　　PACS number(s): 61.30.Gd, 61.30.Cz, 61.30.Pq, 61.30.Hn

I. INTRODUCTION

Lattice simulations where a small cluster of neighboring molecules is represented simply by a headless vector (spin) have been employed in investigating orientational properties of liquid crystals since the pioneering work of Lebwohl and Lasher [1]. Simple lattice models are particularly useful for the investigation of confined systems [2] and complex geometries, where the analytical treatment with the elastic theory may be prohibitive and sometimes has to be restricted to a few approximate situations [3]. In these cases, potentially relevant from the applicative point of view, lattice simulations employing suitable chosen potentials are helpful and can be implemented in a very efficient way [4,5]. Likewise, the study of defects is particularly suitable to being attacked by computer simulations [6,7]. The aim of the present paper is to use Monte Carlo simulations to investigate the role of the elastic anisotropy on the spontaneous deformations of nematic liquid crystals trapped between two concentric cylinders. Systems of this type can be relevant for tribological applications [8–10], where a change in the viscosity and friction properties of a liquid crystal depend on a variation of its molecular organization, and can be also important in photonics in which the confinement of power is improved in clad liquid crystal optical fibers [11–13]. Some special cases have been investigated analytically by many authors [14–21]. Various features of nematics confined between two coaxial cylinders have also been studied by computer simulations [22–25]. Here we have used a Hamiltonian that takes into account the elastic anisotropies as parameters to analyze the dependence of the spontaneous deformations of the nematic

on the relative strengths of these elastic constants and other system variables such as the radii of the cylinders. After a brief description of the simulation model, we present Monte Carlo results obtained for some values of the ratio between bulk elastic constants as well as some values of the thickness of the sample. In addition to quantitative observables, we have also simulated the different polarized microscopy optical patterns that can be expected for the different cases represented by the choice of the parameter values.

II. SIMULATION DETAILS

The sample cell is the annular region between two concentric cylinders, aligned along the **Z** direction, which is filled with nematic liquid crystals. To represent the particles of the uniaxial system to be simulated, N three-dimensional spins $\mathbf{u}_i$ are placed at the sites of a simple cubic lattice and usual periodic boundary conditions are considered along the **Z** direction. The radial boundary conditions are imposed by using two sets of ghost spins, which are kept fixed during the simulations. These sets are built by collecting all the spins that are at distances r_1 and r_2 (largest integer) from the cylinder axes, giving rise to the boundary surfaces S_1 and S_2. In both surfaces, the ghost spins are oriented along the radial **R** direction. The spins in the annular region inside the surfaces F are free to reorient in any direction. The Hamiltonian of the system has the form

$$U = \frac{1}{2} \sum_{\substack{i,j \in F \\ i \neq j}} \Phi_{ij}^B + J_1 \sum_{\substack{i \in F \\ j \in S_1}} \Phi_{ij}^{S_1} + J_2 \sum_{\substack{i \in F \\ j \in S_2}} \Phi_{ij}^{S_2}, \qquad (1)$$

where the first term Φ_{ij}^B refers to the bulk spin-spin interaction and the second and third terms $\Phi_{ij}^{S_1}$ and $\Phi_{ij}^{S_2}$ refer to spin

---

*Corresponding author: rodolfosouza@utfpr.edu.br

interaction with the internal and external surfaces, respectively. In addition, J_i is the ratio between the strength of the interaction with the surface and the strength of the bulk interaction. For simplicity, in the calculations performed in this paper these values are assumed to be $J_1 = J_2 = 1$.

On the surfaces, a Lebwohl-Lasher (LL) [1] pair potential between the spins is assumed in order to represent an anisotropic interaction such as the well-known Rapini-Papoular approximation [26]. Thus, the interaction of the molecules with the surfaces may be governed by a potential of the form

$$\Phi_{ij}^{S_{1,2}} = -P_2(b_{ij}), \tag{2}$$

where $b_{ij} = \mathbf{u}_i \cdot \mathbf{u}_j$ and P_2 is a second-rank Legendre polynomial.

To account for the elastic anisotropy effects, the bulk interaction is assumed to be governed by the pair potential proposed by Gruhn and Hess [27] and extensively applied in computer simulations by Romano and Luckhurst [28–30], known as the GHRL potential. It has the form

$$\Phi_{ij}^{B} = \epsilon_{ij} \{ \lambda [P_2(a_j) + P_2(a_k)] + \mu [a_j a_k b_{jk} - 1/9] \\ + \nu P_2(b_{jk}) + \rho [P_2(aj) + P_2(a_k)] P_2(b_{jk}) \}, \tag{3}$$

where $\epsilon_{ij} = 1$ if i and j are nearest neighbors and 0 otherwise. The scalars a_i and a_j are defined as $a_i = \mathbf{u}_i \cdot \mathbf{s}$ and $a_j = \mathbf{u}_j \cdot \mathbf{s}$, where $\mathbf{s} = \mathbf{r}/|\mathbf{r}|$ and $\mathbf{r} = \mathbf{x}_i - \mathbf{x}_j$, with $\mathbf{x}_i$ and $\mathbf{x}_j$ being dimensionless coordinates of the ith and jth lattice points, respectively. The parameters of the potential may be written as [27]

$$\begin{aligned} \lambda &= \tfrac{1}{3}\Lambda(2K_{11} - 3K_{22} + K_{33}), \\ \mu &= 3\Lambda(K_{22} - K_{11}), \\ \nu &= \tfrac{1}{3}\Lambda(K_{11} - 3K_{22} - K_{33}), \\ \rho &= \tfrac{1}{3}\Lambda(K_{11} - K_{33}), \end{aligned} \tag{4}$$

where Λ is the length of the lattice unit cell. All the parameters are scaled with $|\nu|$, which allows one to recover the LL approximation when $K_{11} = K_{22} = K_{33}$. This potential enables us to rescale the elastic constants with one of them (K_{33}, for instance), while the parameters λ, μ, and ρ remain unchanged. Thus, hereafter the elastic constants will be scaled as K_{11}/K_{33} and K_{22}/K_{33}.

The initial condition corresponds to a sample aligned along the $\mathbf{R}$ direction. The simulation technique is the standard Metropolis Monte Carlo procedure [31]. A spin i in F is randomly selected and an angular move is performed. The move is accepted with probability $p = \min[1, \exp(-\Delta E/k_B T)]$, where k_B is the Boltzmann constant, T is the absolute temperature, and ΔE is the energy difference between the new sample configuration and the old one. The angular move is attempted by applying a rotation of an angle α to one of the axes, randomly chosen. The angle α is fixed at the beginning of the simulations as $\pi/2$ and it is adjusted during the running in order to keep the percentage of the accepted moves around 50%. One Monte Carlo cycle is completed when all the molecules in F have attempted to move once.

To investigate the molecular orientation in the sample, several parameters are evaluated during the simulations. The ordinary second-rank orientational order parameter, defined as

$$\langle P_2 \rangle = \tfrac{3}{2}\langle \cos^2 \beta \rangle - \tfrac{1}{2}, \tag{5}$$

with β representing the angle formed by one spin and a hypothetical global nematic director of the sample, can be obtained by taking the highest eigenvalue of the matrix:

$$Q_{kl} = \frac{3}{2N} \sum_{i=1}^{N} \left(u_{ik} u_{il} - \frac{1}{3}\delta_{kl} \right),$$

where u_{ik} is the component k of the spin i. This parameter may often be inadequate for inhomogeneous or confined systems. For instance, if the sample has a uniform radial orientation, it assumes a value around 0.25, which is equal to its value in the case of a completely disordered two-dimensional system. Therefore, we also find it useful to determine an order parameter with respect to a certain specific direction $\mathbf{c}$, defined as

$$P_{2c} = \frac{3}{2N} \sum_{i=1}^{N} \left((\mathbf{u}_i \cdot \mathbf{c})^2 - \frac{1}{3} \right).$$

This value tends to 1 if the spins are parallel to $\mathbf{c}$ and tends to $-1/2$ if the spins are perpendicular to it. In the present calculations, $\mathbf{c}$ will assume in turn the direction of $\mathbf{R}$, $\mathbf{Z}$, and $\boldsymbol{\theta}$, which are the unit vectors defining the usual cylindrical coordinate system [32].

The simulations allow one to reproduce or predict experimental observations of liquid crystals such as the polarized microscopy optical textures. These patterns can be simulated by means of a Müller matrix approach [7,33], assuming that the molecular domains represented by the spins act as retarders on the light propagating through the sample [34]. The procedure is described in Ref. [35] and the following parameters were employed for computing the optical textures: sample thickness $d = 5.3$ μm, ordinary and extraordinary refractive indices $n_o = 1.5$ and $n_e = 1.66$, respectively, and light wavelength $\lambda_0 = 545$ nm.

For all the cases analyzed here, the reduced temperature, defined as $T_R = k_B T/|\nu|$, was set at $T_R = 0.2$, far enough from the nematic-isotropic transition in the bulk, which is $T_R = 1.1232$ [36] for the Lebwohl-Lasher model. At this low temperature we expect the Monte Carlo simulation to give results similar to those that would be obtained by numerical minimization of the Frank elastic energy, but without the limits on sample size.

III. RESULTS

We focus on analyzing the effects of changing the elastic constants on the spontaneous deformations in this particular cylindrical sample. To accomplish this task, different sets of elastic constants were considered. The height of the cylinders studied was taken to be constant (ten layers with periodic boundary conditions). The external radius used was $r_2 = 40$ (lattice units), but the value $r_2 = 60$ (lattice units) was also considered in order to control possible finite-size effects connected to the external surface. The effects of thickness were instead studied by changing the values of the inner cylinder radius. For each set of elastic constant and cylinder sizes, the simulations were started with all the spins parallel to the $\mathbf{R}$ direction and were allowed to evolve for 10^6 Monte Carlo cycles. A few cases have been followed for longer time to check
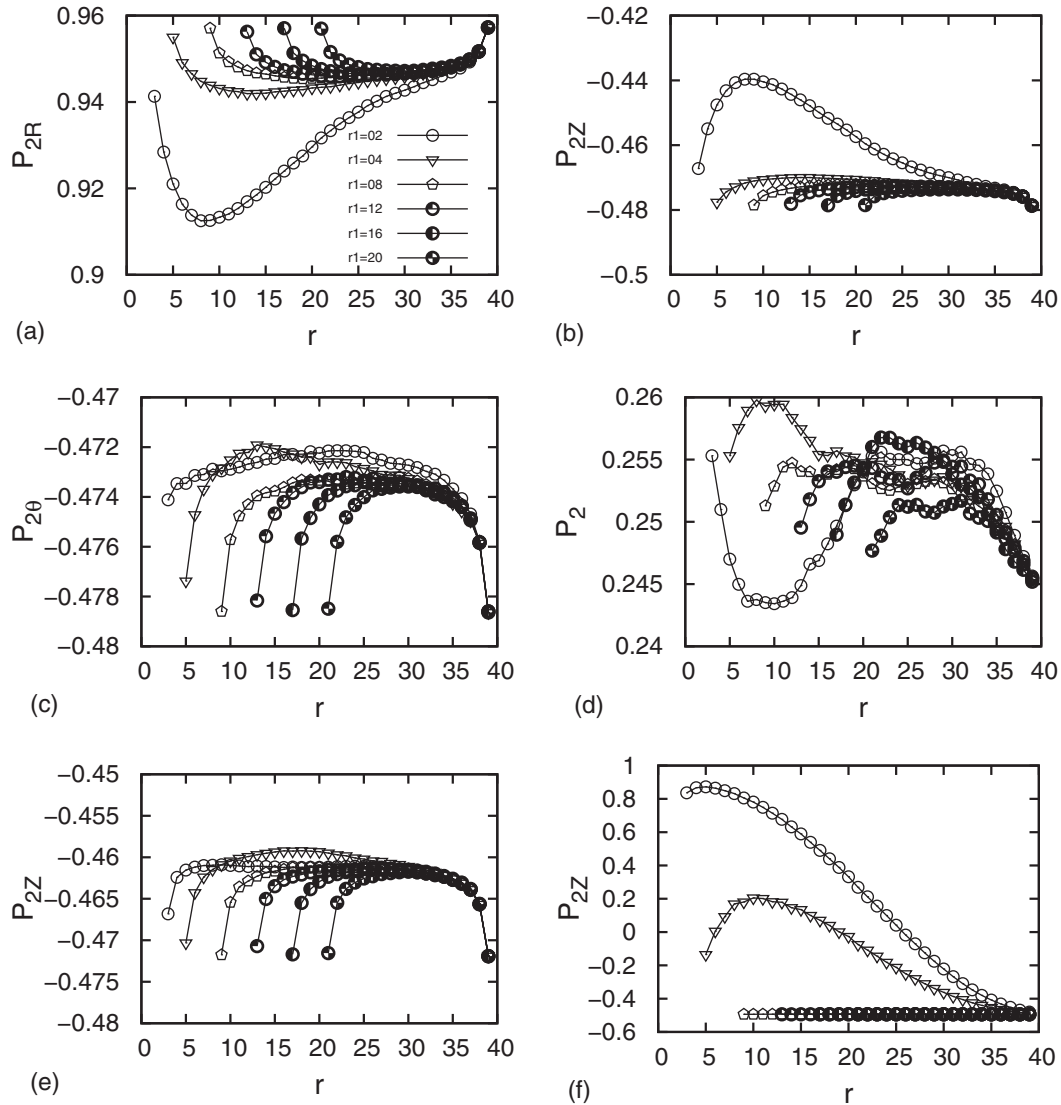
FIG. 1. Profiles for equal elastic constants (LL model) of (a) P_{2R}, (b) P_{2Z}, (c) $P_{2\theta}$, and (d) P_2 as a function of the distance from the cylinder axis for various inner cylinder radii r_1 boundaries. The maximum observed in P_{2Z} has a minimum correspondent in P_{2R}, but no change in $P_{2\theta}$ is detected. The P_2 profiles present values very close to 0.25. Profiles for different elastic constants (GHLR model) of P_{2Z} as a function of the distance from the cylinder axis for the sets (e) $K_{11}/K_{33} = 0.5$ and $K_{22}/K_{33} = 1.0$ and (f) $K_{11}/K_{33} = 3.0$ and $K_{22}/K_{33} = 1.0$. In the latter case, a more evident maximum is observed for P_{2Z} for a larger value of the scaled splay elastic constant.

the stability of the state. The mean value of the parameters were monitored to check if the equilibrium state had been reached. In general, the profiles were practically unchanged after 5×10^5 of these cycles.

In the first case to be considered, all the elastic constants are alike. Thus, the potential given in Eq. (3) reduces to the Lebwohl-Lasher one. Simulation data with the LL model are presented in Figs. 1(a)–1(d) for several values of the inner radius. The cylinders' gap is divided into r_2 bins of a specific thickness. This causes a greater statistical error in the inner bins. We estimate the worst case error to be around 7%. We observe that the values of the orientational order parameters P_{2R}, P_{2Z}, and $P_{2\theta}$ are very close to their imposed surface boundary values, except for the lowest value of the internal radius studied, $r_1 = 2$, in which a small but noticeable (∼10%) deformation appears in the **Z** direction. In that case, while practically the whole sample has a radial configuration,

a small region has a more prominent deformation in the direction of the **Z** axis. This phenomenon is known as escape to the third dimension, or a Fréedericksz-like transition [15]. This increase of order in the **Z** direction is accompanied by a decrease in order along the **R** direction. However, the order in θ remains unchanged. The values of P_2 are very close to that of total disorder in two dimensions, i.e., around $1/4$.

The results are slightly different for lower values of the ratio K_{11}/K_{33}. In this case, no major deformation is observed in all cases, as shown in the data presented in Fig. 1(e), where it is possible to note the absence of a pronounced maximum of the order parameter along the **Z** direction. Since a similar profile is found for the order parameter along the **R** and θ directions, these plots are omitted.

On the other hand, for larger values of the ratio K_{11}/K_{33} the spontaneous deformations become more evident, as shown in Fig. 1(f). However, large deformations emerge only in
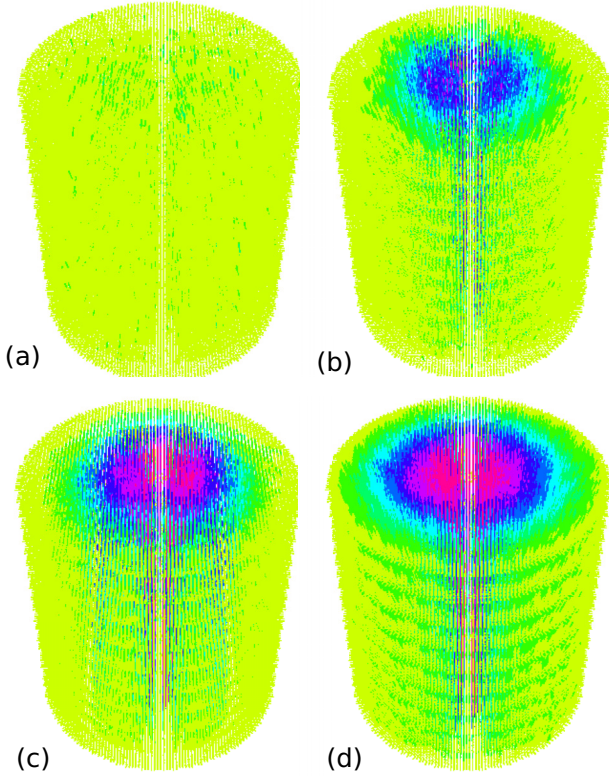
FIG. 2. (Color online) Snapshots of the configuration of the spins at the end of the simulations for $r_1 = 4$, $K_{22}/K_{33} = 1.0$, and (a) $K_{11}/K_{33} = 1$, (b) $K_{11}/K_{33} = 2.0$, (c) $K_{11}/K_{33} = 3$, and (d) $K_{11}/K_{33} = 3.5$. We can verify that there are significant deformations only for high values of the ratio K_{11}/K_{33}. These deformations are more concentrated near the inner cylinder and their size increase as K_{11}/K_{33} increases.
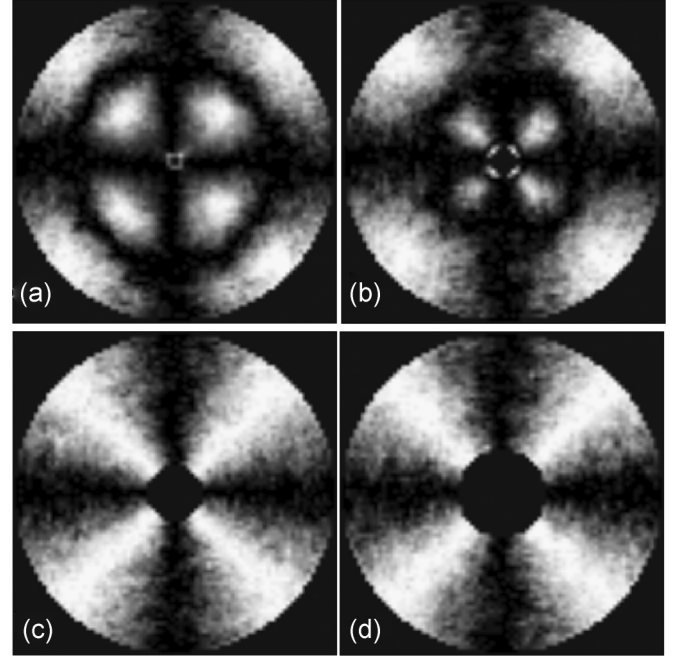

FIG. 3. Microscopic texture between linear crossed polarizers for $K_{11}/K_{33} = 3.0$ and $K_{22}/K_{33} = 1.0$ for a few values of inner radius (a) $r_1 = 2$, (b) $r_1 = 4$, (c) $r_1 = 8$, and (d) $r_1 = 12$. The circular dark rings indicate the presence of a deformation in the **Z** direction.

the **Z** direction, while in the polar plane the spins remain parallel to **R**. Even in this case, no deformation is observed in the θ direction. Despite theoretical results indicating the possibility of observing spontaneous deformations in the θ direction, when K_{11}/K_{33} is higher than a critical value [21], the deformations along **Z** are energetically favorable. This statement can be checked by comparing the energy of two small deformations, one along θ and another one along **Z**, showing that the latter is the lowest one.

These results can also be checked by observing Fig. 2, with colored snapshots for two different values of the ratio K_{11}/K_{33}. The color scheme corresponds to yellow for small values of the component parallel to **Z**, blue for higher values, and shades of red near unity. No distortion is observed for $K_{11}/K_{33} = 1.0$, while strong deformations are observed for higher values for the scaled splay elastic constant.

Another qualitative way to visualize the deformations is to observe the simulated polarized light microscopy textures. Here we assume the direction of the incoming light to be along **Z** with transmission observed between crossed polarizers. Figure 3 shows the textures obtained for a set of values of the inner radius, in the case where $K_{11}/K_{33} = 3.0$ and $K_{22}/K_{33} = 1.0$. One can verify that the escape to the third dimension strongly affects the textures of the sample. Another

conspicuous feature is the lack of deformation in the direction of θ. Deformation in this direction would cause the dark spots to deviate to the right or left, as noted in Ref. [19], which is not observed for these textures.

Although the data indicate that the distortions remain only in the *R-Z* plane and there is no indication of twist distortion on the results, the constant K_{22} seems to have a crucial role in the deformation, as can be seen in Fig. 4. One can verify that for values such that no deformations can be found when $K_{22}/K_{33} = 1.0$, no deformations are also observed for $K_{22}/K_{33} = 2.0$, while they are actually observed for $K_{22}/K_{33} = 0.5$. However, even in this case, the spins remain with no θ component, as can be seen in Fig. 4(c).

To promote a more detailed check of the effects of the elastic constant anisotropy on the deformation, simulations with larger sets of elastic constants have been carried out. In each obtained profile, the highest value for the parameters $P_{2\theta}$ and P_{2Z}, defined as $P_{2\theta\text{-max}}$ and $P_{2Z\text{-max}}$, respectively, are considered. As expected, no value significantly greater than -0.5 was found for $P_{2\theta\text{-max}}$; consequently, these plots have been omitted. The profile of $P_{2Z\text{-max}}$ as a function of K_{11}/K_{33} for a few values of K_{22}/K_{33} is shown in Fig. 5(a) for $r_1 = 2$. One clearly observes the presence of a critical value of the elastic constant for which a deformed state becomes stable, which also depends on K_{22}/K_{33}. The data seem to suggest that the critical value of the ratio K_{11}/K_{33} has a nonlinear relation with the ratio K_{22}/K_{33}.

Following the same procedure of taking the maximum values of the order parameters with respect to θ and **Z**, we build the profiles of $P_{Z\text{-max}}$ versus the radius of the inner surface. The results are shown in Fig. 5(b) for a few values of K_{11}/K_{33} when $K_{22}/K_{33} = 1.0$ and in Fig. 5(c) for several values of K_{22}/K_{33}
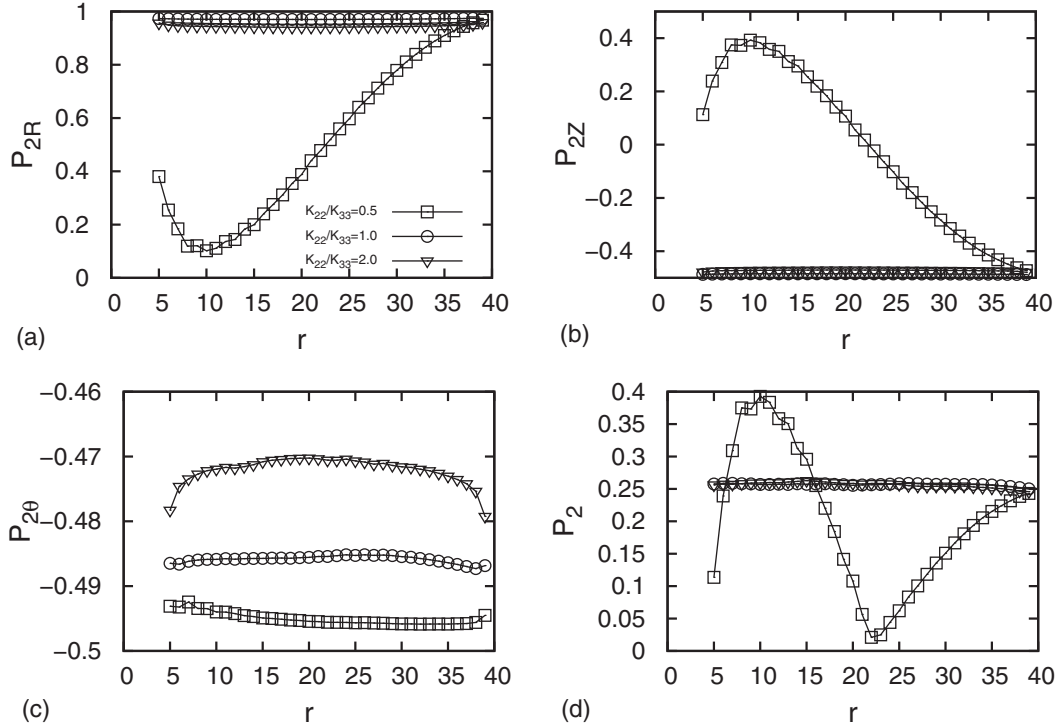
FIG. 4. Profiles of (a) P_{2R}, (b) P_{2Z}, (c) $P_{2\theta}$, and (d) P_2 as a function of the distance from the cylinder axis for $K_{11}/K_{33} = 2.0$, $r_1 = 4$, and a few values of K_{22}/K_{33}. The scaled twist elastic constant seems to induce some relevant deformation parallel to the **Z** axis.
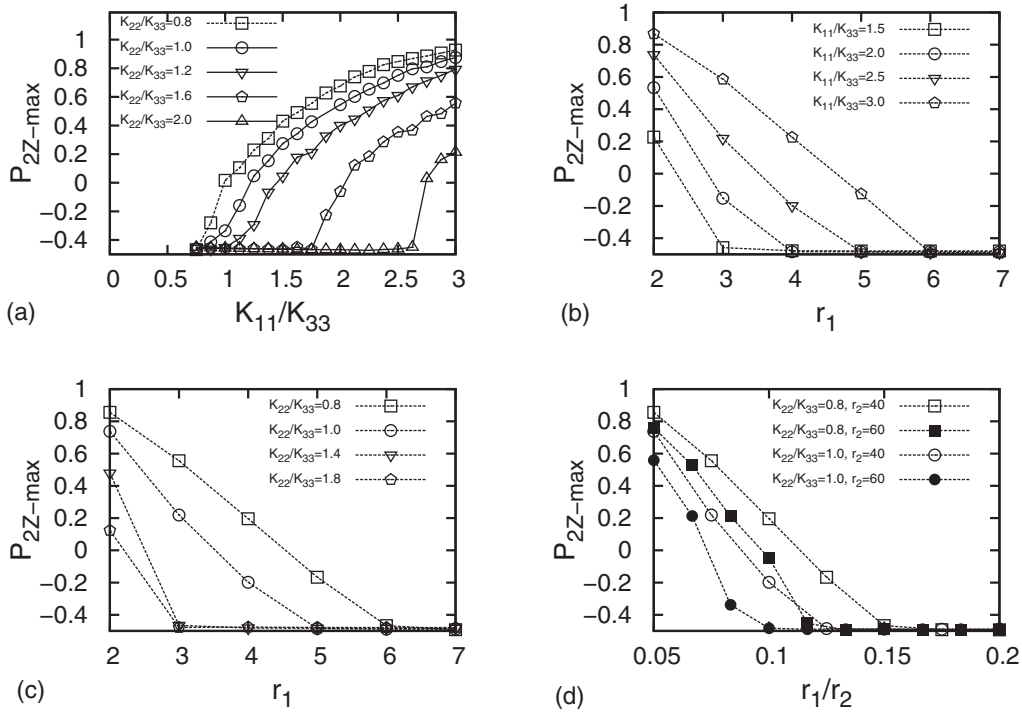

FIG. 5. (a) Maximum amplitude of P_{2Z} ($P_{2Z\text{-max}}$) as a function of the scaled splay elastic constant. A critical behavior is observed for a given ratio K_{11}/K_{33}, which varies according to the values of the scaled twist elastic constant. (b) $P_{2Z\text{-max}}$ as a function of the radius of the inner cylinder for a few values of K_{11}/K_{33} and $K_{22}/K_{33} = 1.0$. (c) $P_{2Z\text{-max}}$ versus the radius of the inner cylinder when $K_{11}/K_{33} = 2.5$ for several values of K_{22}/K_{33}. Both cases indicate that the inner surface can induce the deformation. (d) $P_{2Z\text{-max}}$ as a function of r_1/r_2 for two sets of the elastic constant and two values of the radius of the external cylinder. This plot suggests that, in contrast to predictions from the elastic theory, the Fréedericksz-like transition may depend on the absolute values of the radius of the surfaces.

when $K_{11}/K_{33} = 2.5$. In the theoretical work of Williams and Halperin [15], the authors determine a relation for the set of parameters for which one can find a deformed configuration, namely, $r_2/r_1 = \exp(\pi/\sqrt{K_{11}/K_{33}})$. Similar results have been found recently [21] for a transition along the θ direction. Both results show that the dependence of the spontaneous deformation on the dimension of the sample relies only on the ratio r_2/r_1 and not on the absolute values of r_2 and r_1. In order to verify this, we have carried out other simulations by assuming $r_2 = 60$. The results are shown in Fig. 5(d), where the maximum values of P_{2Z} are plotted as a function of r_1/r_2 for two different values of K_{11}/K_{33} and for two different values of r_2 (40 and 60). Since the obtained profiles are quite different, the resulting plot suggests that the absolute values of the radius defining the cylindrical region representing the cell also play a role in the appearance of deformations. The simulations show for $r_1/r_2 < 0.15$ a dependence on the absolute values of the radius of the cylinders rather than just on the ratio and a more pronounced dependence on the elastic anisotropy. Indeed, the elastic anisotropy affects the value of the parameter Λ, which in turn is connected to the size of the system. Thus, this behavior, not predicted by the elastic theory of Williams and Halperin [15], may be connected not only to the peculiarities of the GHRL potential but also to the relative small size of the system. One of the advantages of our treatment is the possibility to go to the nanoscale, i.e., below the continuum. For very small ratios r_1/r_2, the results may be affected by the small number of spins used to mimic the inner cylinder, which for $r_2 = 60$ results in $r_1 < 5$, a scale where the deviations from continuum are not surprising. Preliminary investigations dealing with larger values of the external radius seem to indicate that the elastic limit is attained for much large samples, as expected.

This dependence of the deformations on the cylinder radius is indeed quite reasonable because the number of spins that are oriented radially is small compared to that of bulk spins. Therefore, the order is maintained only for a few lattice units when one moves away from the surfaces. A perhaps surprising result instead is the observation of a dependence on the scaled twist elastic constant, even if the no twist deformation is found. Since the deformations depend on the absolute values of the cylinders radius, the parameter Λ also has some importance. This happens because Λ can be written as $\Lambda = 3\nu/|K_{11} - 3K_{22} - K_{33}|$. Thus, it changes according to the elastic constant values. This implies that, for each set of elastic constants, the length of the unit cell also changes.

IV. CONCLUSION

We have performed Monte Carlo simulations to investigate the role of the elastic anisotropy in the spontaneous deformation of a nematic liquid crystal confined to the gap between concentric cylinders whose facing surfaces impose homeotropic boundaries. We focused on the effect of the elastic anisotropy on the onset of spontaneous deformation by changing the values of the bulk elastic constants of splay, twist, and bend. When these constants are similar, we have found that a prominent deformation along the cylinder axis exists, but is confined to a small region, while practically the whole sample has a radial configuration. For the cases in which $K_{22} = K_{33}$, with a small enough value for the ratio K_{11}/K_{33}, we observed that all the spins in the bulk follow the orientation imposed by the surface. In contrast, for larger values of the ratio K_{11}/K_{33} conspicuous spontaneous deformations arose perpendicular to the polar plane. Snapshots and microscopic polarized texture confirm the presence of the director deformation close to the inner surface. In addition, we observed that these deformations are also dependent on the ratio K_{22}/K_{33} and on the specific values of the radius of each cylindric surface (not only on the ratio r_1/r_2, as theoretically predicted). Finally, it is worth mentioning that even if twist deformation was not found in the simulations, the other results were dependent on the scaled twist elastic constant. This dependence seems to have its source in the parameter Λ used here to represent the length of the unit cell.

[1] P. A. Lebwohl and G. Lasher, Phys. Rev. A **6**, 426 (1972).

[2] P. Pasini, C. Chiccoli, and C. Zannoni, in *Advances in the Simulations of Liquid Crystals*, edited by P. Pasini and C. Zannoni (Kluwer Academic, Dordrecht, 2000).

[3] G. Barbero and L. R. Evangelista, *An Elementary Course on the Continuum Theory for Nematic Liquid Crystals* (World Scientific, Singapore, 2001).

[4] C. Chiccoli, P. Pasini, F. Semeria, and C. Zannoni, Mol. Cryst. Liq. Cryst. **212**, 197 (1992).

[5] C. Chiccoli, I. Feruli, O. D. Lavrentovich, P. Pasini, S. V. Shiyanovskii, and C. Zannoni, Phys. Rev. E **66**, 030701 (2002).

[6] See, e.g., *Defects in Liquid Crystals: Computer Simulations, Theory and Experiment*, edited by O. D. Lavrentovich, P. Pasini, C. Zannoni, and S. Zumer (Kluwer Academic, Dordrecht, 2001).

[7] C. Chiccoli, O. D. Lavrentovich, P. Pasini, and C. Zannoni, Phys. Rev. Lett. **79**, 4401 (1997).

[8] G. Biresaw, *Tribology and the Liquid-Crystalline State*, ACS Symposium Series No. 441 (ACS, Washington, DC, 1990).

[9] B. I. Kupchinov, J. Frict. Wear **30**, 169 (2009).

[10] T. Amann, C. Dold, and A. Kailer, Tribol. Int. **65**, 3 (2013).

[11] S. Chen and T. J. Chen, Appl. Phys. Lett. **64**, 1893 (1994).

[12] P. K. Choudhury, Prog. Electromagn. Res. **131**, 169 (2012).

[13] M. Ghasemi and P. K. Choudhury, J. Nanophoton. **8**, 083997 (2014).

[14] H. Tsuru, J. Phys. Soc. Jpn. **59**, 1600 (1990).

[15] D. R. M. Williams and A. Halperin, Phys. Rev. E **48**, R2366 (1993).

[16] D. R. M. Williams, Phys. Rev. E **50**, 1686 (1994).

[17] A. Corella-Madueño, A. Castellanos-Moreno, S. Gutiérrez-López, R. A. Rosas, and J. A. Reyes, Phys. Rev. E **78**, 022701 (2008).

[18] I. V. Kotov, M. V. Khazimullin, and A. P. Krekhova, Mol. Cryst. Liq. Cryst. **366**, 885 (2001).

[19] C. A. R. Yednak, R. Teixeira de Souza, G. G. Lenzi, E. K. Lenzi, and L. R. Evangelista, Mol. Cryst. Liq. Cryst. **526**, 82 (2010).

[20] G. Bevilacqua and G. Napoli, Phys. Rev. E **81**, 031707 (2010).

[21] R. Teixeira de Souza, J. C. Dias, R. S. Mendes, and L. R. Evangelista, Physica A **389**, 945 (2010).

[22] G. Sai Preeti, V. Vijay Kumar, V. S. S. Sastry, and K. P. N. Murthy, Comput. Mater. Sci. **44**, 180 (2008).

[23] V. Zakharov, A. A. Vakulenko, and S. Romano, J. Chem. Phys. **132**, 094901 (2010).

[24] C. Chiccoli, P. Pasini, R. Teixeira de Souza, L. R. Evangelista and C. Zannoni, Phys. Rev. E **84**, 041705 (2011).

[25] C. Chiccoli, P. Pasini, L. R. Evangelista, R. Teixeira de Souza, and C. Zannoni, Mol. Cryst. Liq. Cryst **576**, 42 (2013).

[26] A. Rapini and M. Papoular, J. Phys. Colloques **30**, C4-54 (1969).

[27] T. Gruhn and S. Hess, Z. Naturforsch. A **51**, 1 (1996).

[28] S. Romano, Int. J. Mod. Phys. B **12**, 2305 (1998).

[29] S. Romano, Phys. Lett. A **302**, 203 (2002).

[30] G. R. Luckhurst and S. Romano, Liq. Cryst. **26**, 871 (1999).

[31] N. Metropolis, A. W. Rosenbluth, M. N. Rosenbluth, A. H. Teller, and E. Teller, J. Chem. Phys. **21**, 1087 (1953).

[32] *CRC Standard Mathematical Tables and Formulae*, edited by D. Zwillinger (Chapman & Hall/CRC, Boca Raton, 2003).

[33] A. Killian, Liq. Cryst. **14**, 1189 (1993).

[34] R. Ondris-Crawford, E. P. Boyko, B. G. Wagner, J. H. Erdmann, S. Žumer, and J. W. Doane, J. Appl. Phys **69**, 6380 (1991).

[35] E. Berggren, C. Zannoni, C. Chiccoli, P. Pasini, and F. Semeria, Phys. Rev. E **50**, 2929 (1994).

[36] U. Fabbri and C. Zannoni, Mol. Phys. **58**, 763 (1986).